Safety Analysis of Long-Range and High-Power Wireless Power Transfer Using Resonant Beam

Wen Fang, Hao Deng, Qingwen Liu, *Senior Member, IEEE*, Mingqing Liu, Qingwei Jiang, Liuqing Yang, *Fellow, IEEE*, and Georgios B. Giannakis, *Fellow, IEEE*

***Abstract*—Resonant Beam Charging (RBC) is a promising Wireless Power Transfer (WPT) technology to realize long-range and high-power charging for electronic devices. However, the safety mechanism of the RBC system has not been investigated so far. In this paper, we propose an analytical model based on electromagnetic field analysis for evaluating the performance of the RBC system with external object invasion, such as the benchmark for the WPT safety, irradiance on the invading object. For the RBC system with 5 m transmission distance and 1 W output electric power, the safety numerical analysis of radiation illustrates that the maximum irradiance on the invading object is 0.81 W/cm^2, which is approximately $1/10$ compared with 8.22 W/cm^2 for the comparable laser charging system. Particularly, the peak irradiance on the invading object of the RBC system satisfies the Maximum Permissible Exposure (MPE) requirement for human skin, which is 1 W/cm^2 in the standard "Safety of Laser Products IEC 60825 − 1". Hence, the RBC system can realize skin-safe WPT with Watt-level power over meter-level distance.**

***Index Terms*—Electromagnetic field analysis, resonant beam charging, wireless power transfer, inherent safety.**

I. Introduction

THE rapid development of the Internet of Things (IoT) and the new-generation communication technology faces the challenges of insufficient device endurance and inconvenient wired power supply [1]. For example, IoT devices such as the Unmanned Aerial Vehicle (UAV) cannot operate for a long time due to battery limitations [2]. Hence, Wireless Power Transfer (WPT) technology has become an attractive solution for the power supply recently [3]. However, the existing WPT technologies are difficult to ensure safety while realizing long-range and high-power transfer. For instance, induction coupling and magnetic resonance WPT face safety challenges due to electromagnetic field leakage from coils [4]; while laser and radio frequency WPT have safety issues with the direct irradiation of external object [5], [6].

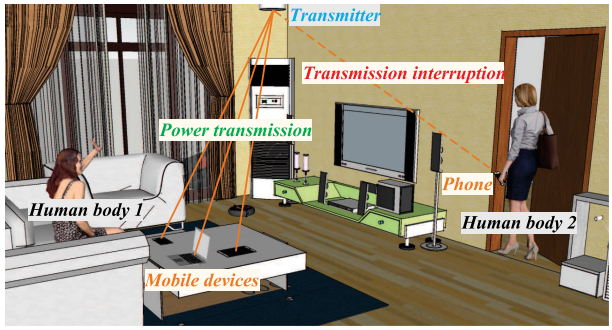

Fig. 1. A typical RBC application scenario.

Recently, many research works on improving WPT safety have been reported. A Living Object Detection (LOD) system based on comb pattern capacitive sensor is proposed in [7], which shows that the magnetic radiation can be suppressed if a living object is placed in the transmission channel. [8] illustrates a WPT system based on ultra-wideband retro-reflective beamforming, which leads to little hazard/interference to other objects. A novel laser WPT system with a low-power guard ring laser is presented in [9], which provides a feedback mechanism to trigger the shutter for turning off the beam quickly, whenever a human approaches the path of the high-power laser. However, these designs all rely on passive protective techniques rather than the inherent mechanism of the WPT system.

Resonant Beam Charging (RBC, also known as Distribution laser charging, DLC) is proposed in [10], [11] for long-range and high-power WPT. The RBC system is based on an open-cavity laser, and the resonant beam in the resonant cavity is used to transfer energy from transmitter to receiver. The system architecture and power transfer process of the RBC system are studied in [12], while the efficiency optimization and resource allocation are investigated in [13], [14].

The typical application scenario of the RBC system is shown in Fig. 1. The human body 1 away from the transmission path will nearly not be exposed to the radiation of resonant beam, since most of the energy (nearly 100%) is stored in the directional resonant beam [15]. However, if an external object (an object outside

Manuscript received November 6, 2020; revised February 27, 2021 and April 9, 2021; accepted April 19, 2021. Date of publication May 3, 2021; date of current version May 28, 2021. The associate editor coordinating the review of this manuscript and approving it for publication was Dr. An Liu. This work was supported in part by the National Key R&D Program of China under Grants 2020YFB2103900 and 2020YFB2103902, and in part by the National Natural Science Foundation of China under Grants 61771344 and 62071334. *(Corresponding authors: Qingwen Liu; Hao Deng.)*

Wen Fang, Qingwen Liu, Mingqing Liu, and Qingwei Jiang are with the College of Electronic and Information Engineering, Tongji University, Shanghai 200000, China (e-mail: wen.fang@tongji.edu.cn; qliu@tongji.edu.cn; clare@tongji.edu.cn; jiangqw@tongji.edu.cn).

Hao Deng is with the School of Software Engineering, Tongji University, Shanghai 200000, China (e-mail: denghao1984@tongji.edu.cn).

Liuqing Yang is with the Department of Electrical and Computer Engineering, University of Minnesota, Minneapolis, MN 55455 USA (e-mail: qingqing@umn.edu).

Georgios B. Giannakis is with the Digital Technology Center and the Department of Electrical and Computer Engineering, University of Minnesota, Minneapolis, MN 55455 USA (e-mail: georgios@umn.edu).

Digital Object Identifier 10.1109/TSP.2021.3076893

the cavity, such as a living object) invades the resonant cavity, the resonant beam is diminished and interrupted immediately since the resonant beam path is blocked. For example, the human body 2 in Fig. 1 blocks the resonant beam between the transmitter and the phone embedded with a receiver, so the resonant beam is interrupted. Afterwards, the energy transmission is suspended. That is, the RBC system enables safe wireless power transfer. However, the RBC safety mechanism has only a qualitative description and lacks quantitative evaluation so far.

The resonant beam is the intra-cavity laser, and resonant beam radiation is a kind of electromagnetic radiation [10]. The safety of RBC system should comply with the requirements of "Safety of laser products IEC $60825-1$" [16]. That is, in a safe RBC system, the irradiance on the invading object must be less than the Maximum Permissible Exposure (MPE, the level of laser radiation to which, under normal circumstances, persons may be exposed without suffering adverse effects, unit: W/cm^2) of skin. Thus, we investigate here the safety mechanism of RBC system and analyze the irradiance on the external object invading into the resonant cavity based on a signal processing technology, i.e., electromagnetic field analysis since the electromagnetic field is the signal in electronics and telecommunications [17], [18].

In this paper, at first, we introduce the RBC system architecture and depict the dynamic response mechanism for external object invasion. Then, we establish an analytical model combing electromagnetic field analysis and circulating power model to calculate the irradiance on the invading object. Afterwards, we numerically analyze the effects of external object invasion on output power and irradiance to determine the safety level of the RBC system according to the laser safety standards IEC $60825-1$. Finally, we compare RBC system with laser charging system under the same invasion conditions to highlight RBC's superior inherent safety. The contributions of this paper include:

c1) We propose an analytical model, which combines the electromagnetic field analysis and the circulating power model, for evaluating the performance of the RBC system with external object invasion. It quantitatively reveals the inherent safety mechanism of the RBC system.

c2) Based on the analytical model, the amplitude distribution at any plane in the resonant cavity, output beam and electric power, and the irradiance on the external object can be calculated through the safety numerical analysis of radiation.

c3) We numerically analyze the radiation of the RBC system based on a Fabry-Pérot (FP) cavity with 6 mm radius reflectors. The results show that it can realize skin-safe, 5 m-distance, and 1 W-power WPT. Moreover, its maximum irradiance is only $1/10$ of the comparable laser charging system.

In the rest of this paper, we introduce the RBC system architecture and illustrate the response mechanism of RBC system for external object invasion in Section II. In Section III, we establish an analytical model based on electromagnetic field analysis to calculate irradiance on the invading object. Afterwards, we demonstrate the changes in output power and irradiance with external object invasion, determine the safety level of the RBC system, and compare the irradiance on invading object of the RBC system to that of the laser charging system in Section IV. Finally, we make a conclusion along with the future research in Section V.

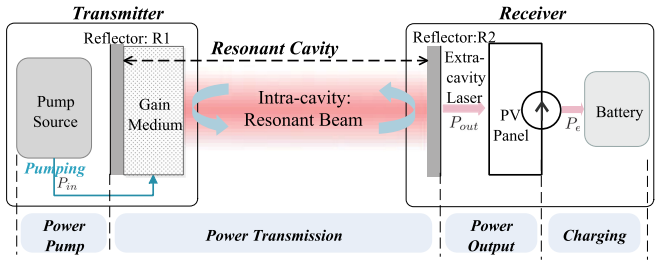

Fig. 2. RBC structure.

II. Problem Statement

RBC is a promising technology to achieve safe, high-power, and long-range WPT. At first, we present the structure of RBC system to illustrate its WPT characteristics. Afterwards, we illustrate the response mechanism of external object invasion and describe the inherent safety study mathematically.

A. Resonant Beam Charging System

As depicted in Fig. 2, the RBC system consists of a transmitter and a receiver. The transmitter and receiver are separated spatially to form a resonator. The resonant beam generated within the resonator acts as the carrier to transfer energy in free space.

The transmitter is comprised of a pump source, a reflector $R1$ with high reflectivity, and a gain medium. The receiver consists of a reflector $R2$ with low reflectivity, a Photovoltaic (PV) panel, and a battery. During power transfer, a portion of intra-cavity resonant beam is reflected from the reflector $R2$ to the transmitter for gain amplification in the gain medium, while the other portion passes through $R2$ to form the extra-cavity laser. The extra-cavity laser is then converted into electric power by the PV panel for battery charging.

The energy flow in the RBC system is as follows. i) Power Pump: The pump source provides the pump power P_{in} to stimulate out and amplify the resonant beam in the gain medium; ii) Power Transmission: The intra-cavity resonant beam propagates back and forth in free-space, transferring energy from transmitter to receiver; iii) Power Output: The resonant beam passes through the reflector $R2$ with extra-cavity laser power P_{out}, and then is converted into the output electric power P_e by the PV panel; and, iv) Charging: The output electric power P_e is used for charging the battery.

Among the energy flow, the "Power Pump," "Power Output" and "Charging" stages are encapsulated in the transmitter and receiver, almost without the possibility of external object invasion. Therefore, these three stages lead to no safety hazards for the external object. However, during the "Power Transmission" stage, the external object in the free space may invade the resonant beam. Afterwards, the irradiation on the external object by resonant beam will bring safety risks.

According to the principles of laser, the resonant beam is essentially a kind of intra-cavity laser [10]. Therefore,

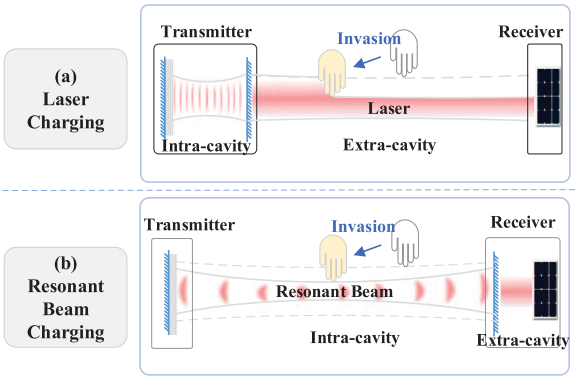

Fig. 3. Comparison of laser charging system and RBC system.

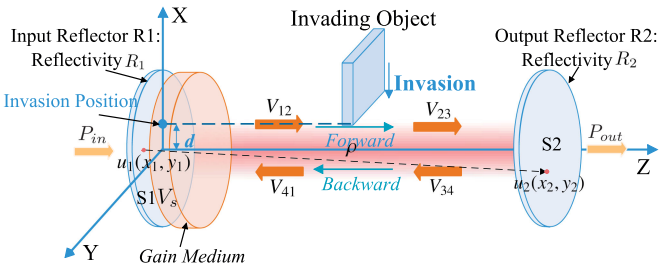

Fig. 4. Schematic diagram of external object invasion in the RBC system.

similar to the laser, the resonant beam has the characteristic of energy-concentrated, which can realize long-range and high-power WPT. As WPT technologies, the difference between RBC and laser charging is depicted in Fig. 3. For laser charging, if an external object invades the transmission path (extra-cavity laser), the intra-cavity resonance will not be affected, and the laser power is continuously transferred (Fig. 3(a)). However, the intra-cavity resonance will stop immediately with object invasion, and then the energy transmission will cease quickly in the RBC system (Fig. 3(b)). This characteristic in RBC system is known as "inherently safe" [10]. Hence, compared to the laser charging system, the external object invading RBC system will be exposed to beam radiation with lower irradiance for a shorter time.

B. Dynamic Response for External Object Invasion

To theoretically analyze the inherent safety and determine the safety level of RBC system, we analyze the response mechanism of external object invasion and explain the problem of determining safety level mathematically.

The schematic diagram of external object invasion in RBC system is shown in Fig. 4. During power transfer, the external object may invade the resonant cavity in any position on the z-axis (connecting line of the center of the input and output reflectors) at any time, which will cause changes in the resonator working states. The dynamic response mechanism of RBC system to external object invasion is illustrated in the following.

The three basic components of a laser resonator are: i) Lasing material, namely the gain medium, ii) Pump source, and, iii) Optical cavity consisting of reflectors to act as the feedback mechanism for light amplification [19], [20]. What's more, the necessary condition of light amplification (i.e., laser generation) is to satisfy the laser threshold condition as [19]

$$g_0\ell = |\ln(\sqrt{R_1R_2\ V}V_s)|, \tag{1}$$

where $g_0\ell$ is the small-signal gain of the gain medium, which increases with the pump power. R_1 and R_2 are the reflectivities of the two reflectors at the transmitter and receiver, respectively. V_s is the transfer factor ($= 1 - \delta$, where δ is the transmission loss) of the gain medium. V represents the transfer factor in a round-trip resonant beam transmission between the transmitter and receiver, which can be obtained by multiplying the transfer factors of four transmission stages: V_{12} (input reflector to invading object plane), V_{23} (invading object plane to output reflector), V_{34} (output reflector to invading object plane), and V_{41} (invading object plane to input reflector).

If there is no external object invasion, the small-signal gain $g_0\ell$ is larger than the laser threshold condition shown in (1) for resonant beam oscillation, and the resonant beam is pumped out stably. While an external object invades the resonant cavity, the propagation loss increases. That is, the transfer factor V decreases to V'. Thus, as the invading object blocks the resonant beam gradually, the laser threshold condition in the resonant cavity is no longer satisfied, i.e.,

$$g_0\ell < |\ln(\sqrt{R_1R_2\ V'}V_s)|. \tag{2}$$

Afterwards, the stimulated amplification process is stopped, and the intra-cavity oscillation is interrupted. Then, the energy transmission is suspended, and the output power P_{out} changes to 0 W.

To reveal whether the RBC system meets the laser safety standard, we will analyze the irradiance I (i.e., radiant intensity, the quotient of the radiant flux incident on an element of a surface by the area of that element, unit: W/cm^2) on the invading object during the invasive process. Referring to the laser safety standard "Safety of laser products IEC $60825-1$," if the irradiance I is below the MPE at a certain level I_{MPE}, that is [16]

$$I < I_{MPE}, \tag{3}$$

the RBC system can be considered as satisfying the corresponding safety level [16].

III. Analytical Model

To analyze the safety of RBC system theoretically and numerically, we need to obtain the irradiance of the resonant beam on the invading object. In this section, we present the use of electromagnetic field computation for beam power intensity distribution analysis firstly [21]. Then, combining the circulating power model, we calculate the irradiance on the object.

Due to the directivity of the beam, the irradiance on the invading object can be approximately represented by the sum of forward (from the input reflector to output reflector) irradiance I^+ and backward (from the output reflector to input reflector) irradiance I^- [19], [20], [22]:

$$I(x, y, z) = \sum_{o\subseteq\{+,-\}} [I^o(x, y, z)]. \tag{4}$$

where (x, y, z) corresponds to the coordinate values of invading object in the spatial cartesian coordinate system depicted in Fig. 4.

With the cartesian coordinate system, the irradiance $I^{\pm}(x, y, z)$ is expressed as the product of the maximum power intensity $I_m^{\pm}(z)$ and normalized power intensity distribution $i^{\pm}(x, y, z)$ on the cross-section at the axial position z in the resonant cavity [23]

$$I^o(x, y, z) = I_m^o(z) i^o(x, y, z), o \subseteq \{+, -\}, \tag{5}$$

where $i^{\pm}(x, y, z)$ is the square of the normalized field distribution $U^{\pm}(x, y, z)$ [23]:

$$i^o(x, y, z) = |U^o(x, y, z)|^2, o \subseteq \{+, -\}. \tag{6}$$

Therefore, to obtain the irradiance on the invading object, the normalized field distribution $U^{\pm}(x, y, z)$ and the maximum power density $I_m^{\pm}(z)$ at the invading position of the object need to be calculated. We investigate here an RBC system with two plane mirror reflectors (i.e., Fabry-Pérot (FP) resonator) and a thin-disk gain medium to obtain irradiance I on the invading object through the "Electromagnetic Field Analysis," "Circulating Power Model," and "Irradiance Calculation Model" in the following.

A. Electromagnetic Field Analysis

To calculate the irradiance on the invading object accurately and dynamically, we explore the electromagnetic field propagation in the resonant cavity based on an external object invasion model. Combining the Fresnel-Kirchhoff diffraction theory, Fast-Fourier-Transform (FFT) method, and Fox-Li numerical iteration algorithm, we can obtain the field distribution on any plane in the resonator.

In the diffraction theory, Huygens-Fresnel principle shows that the vibration of a position in space can be regarded as the coherent superposition of the secondary waves emitted by all the plane elements in front of the wave [24], [25]. Thus, in the FP resonator shown in Fig. 4 without external object invasion, the integral formula of Fresnel-Kirchhoff diffraction is [20], [23]

$$u_2(x_2, y_2) = \frac{j}{\lambda L} \iint_{S1} u_1(x_1, y_1) e^{-jk\rho} ds, \tag{7}$$

where $u_1(x_1, y_1)$ and $u_2(x_2, y_2)$ are the field distribution on the surface of reflectors $R1$ and $R2$ respectively, $S1$ is the plane of $R1$. j is the imaginary unit, λ is the resonant beam wavelength, L is the resonator length, and ρ represents the distance between (x_1, y_1) and (x_2, y_2). k is the wavenumber and can be calculated by [26]

$$k = \frac{2\pi}{\lambda}. \tag{8}$$

The distance ρ between the points $(x_1, y_1, 0)$ on the wave source surface and (x_2, y_2, z) on the observation surface is expressed approximately as [27]

$$\rho \approx z \left[1 + \frac{1}{2} \left(\frac{x_2 - x_1}{z} \right)^2 + \frac{1}{2} \left(\frac{y_2 - y_1}{z} \right)^2 \right], \tag{9}$$

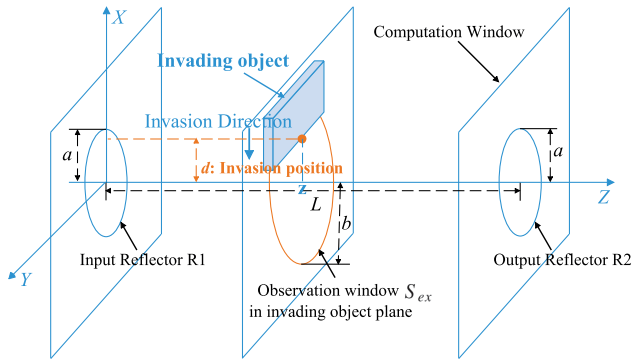

Fig. 5. FFT-based method for electromagnetic field distribution.

where $z = L$. Thus, the formula for calculating the filed distribution on the reflector $R2$ can be derived from (7), (9) and [27]

$$u_2(x_2, y_2) = \frac{j \exp(-jkL)}{\lambda L} \iint_{S_1} u_1(x_1, y_1) \exp\left\{ \frac{-jk}{2L} \left[(x_2 - x_1)^2 + (y_2 - y_1)^2 \right] \right\} ds. \tag{10}$$

The integral formula of Fresnel-Kirchhoff diffraction (10) can be written as the convolution [28]:

$$u_2(x_2, y_2) = u_1(x_1, y_1) \otimes T(x_2, y_2), \tag{11}$$

with

$$T(x_2, y_2) = \frac{j \exp(-jkL)}{\lambda L} \exp\left\{ \frac{-jk}{2L} (x_2^2 + y_2^2) \right\} \tag{12}$$

Besides, the field distribution on a transmission plane is usually expressed as a function of its effective propagation aperture. The relationship between the field distribution $u'(x, y)$ and $u(x, y)$ before and after passing through the plane is [29]

$$u(x, y) = B(x, y) \cdot u'(x, y), \tag{13}$$

where $B(x, y)$ represents the effective propagation aperture on the plane.

As depicted in Fig. 5, with the external object invading the resonant cavity, the Fresnel-Kirchhoff diffraction calculation in (7) can be divided into four stages: from $R1$ to S_{ex}, from S_{ex} to $R2$, from $R2$ to S_{ex}, and from S_{ex} to $R1$. The effective propagation aperture of the reflectors $R1$ and $R2$ is

$$B_R(x, y) = \begin{cases} 1, x^2 + y^2 \le a^2 \\ 0, x^2 + y^2 > a^2 \end{cases}, \tag{14}$$

where a is the radius of the reflectors. In addition, the effective propagation aperture of observation window in the invading object plane S_{ex} is

$$B_{ex}(x, y) = \begin{cases} 1, x^2 + y^2 \le b^2 \text{ and } x \le d \\ 0, x^2 + y^2 > b^2 \text{ or } x > d \end{cases}, \tag{15}$$

where b represents the radius of the observation window S_{ex}, and d is the invasion position of object depicted in Fig. 5.

Then, we adopt Fast-Fourier-Transform (FFT) method for a round-trip field distribution calculation [29]. The initial field distribution of input reflector $R1$ is $u_1'(x_1, y_1)$, then the field

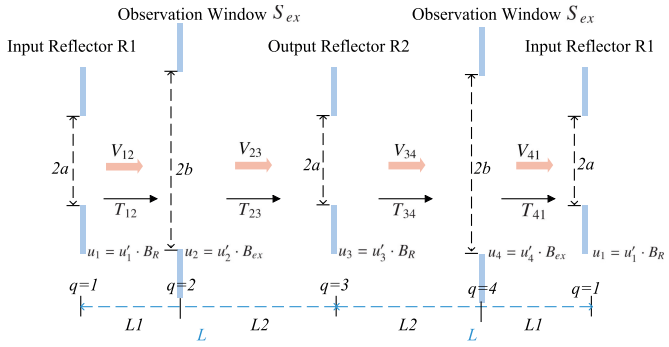

Fig. 6. The electromagnetic field propagation of a round-trip.

distribution propagation during a round-trip shown in Fig. 6 can be derived from (11), (12), (13), (14), (15), and [29] as:

1) From the input reflector to the invading object plane, the field distribution $u_2'(x_2, y_2)$ on S_{ex} is

$$u_2'(x_2, y_2) = \mathscr{F}^{-1}\{\mathscr{F}\{u_1'(x_1, y_1) \cdot B_R(x_1, y_1)\} \cdot \mathscr{F}\{T_{12}(x_2, y_2)\}\}\Delta x_1 \Delta y_1. \tag{16}$$

2) From the invading object plane to the output reflector, the field distribution $u_3'(x_3, y_3)$ on $R2$ is depicted as

$$u_3'(x_3, y_3) = \mathscr{F}^{-1}\{\mathscr{F}\{u_2'(x_2, y_2) \cdot B_{ex}(x_2, y_2)\} \cdot \mathscr{F}\{T_{23}(x_3, y_3)\}\}\Delta x_2 \Delta y_2. \tag{17}$$

3) From the output reflector to the invading object plane, the field distribution $u_4'(x_4, y_4)$ on S_{ex} can be expressed as

$$u_4'(x_4, y_4) = \mathscr{F}^{-1}\{\mathscr{F}\{u_3'(x_3, y_3) \cdot B_R(x_3, y_3)\} \cdot \mathscr{F}\{T_{34}(x_4, y_4)\}\}\Delta x_3 \Delta y_3. \tag{18}$$

4) From the invading object plane to the input reflector, the field distribution $u_1'(x_1, y_1)$ on $R1$ is

$$u_1'(x_1, y_1) = \mathscr{F}^{-1}\{\mathscr{F}\{u_4'(x_4, y_4) \cdot B_{ex}(x_4, y_4)\} \cdot \mathscr{F}\{T_{41}(x_1, y_1)\}\}\Delta x_4 \Delta y_4. \tag{19}$$

where Δx_i and Δy_i $(i \in 1, 2, 3, 4)$ are dimensions of surface elements in the horizontal and vertical coordinate directions.

Then, the field distribution on the invading object plane after a round-trip propagation can be obtained from the above calculation. Afterwards, to obtain a steady field distribution on invading object plane, we adopt the "Fox-Li" numerical iteration method with multiple iterations after plane wave incidence [30]. Each time for diffraction integral calculation of the above four-step propagation is equivalent to one back and forth propagation (i.e., from the input reflector to the input reflector) in the resonant cavity, and the normalization of the previous result is the input of the next calculation. As depicted in Fig. 7, the iteration continues until a self-reproductive mode (i.e., steady field distribution) is generated.

Finally, the normalized power intensity distribution $i(x, y, z)$ on the invading object plane can be derived from (6).

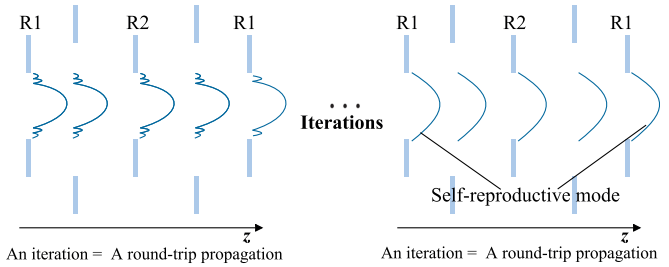

Fig. 7. Iteration continues until the diffraction screens out a self-reproductive mode ("Fox-Li" iteration method).

B. Circulating Power Model

From Fig. 2, the pump power stimulates the gain medium to pump out the resonant beam, then the resonant beam oscillates between the transmitter and the receiver for power transfer. The output beam power can be finally converted into the electric power P_e for battery charging. The end-to-end conversion process is described below.

Firstly, for realizing population inversion and pumping out resonant beam, the pump power P_{in} is converted into the available stimulating power (i.e., power in the upper laser level) inside the gain medium with the excitation efficiency η_{excit}, so the available power P_a can be depicted as [19]

$$P_a = \eta_{\text{excit}} P_{\text{in}}. \tag{20}$$

For the homogeneously broadened lasers, the available stimulating power is determined by its physical properties, that is [19]

$$P_a = g_0 \ell A I_s, \tag{21}$$

where $g_0\ell$ is the small-signal gain, A is the cross-sectional area of the gain medium, and I_s is the saturation intensity, which is a characteristic of the laser material and represents the peak incident light intensity that can be amplified by the gain medium. Thus, it is determined by the physical characteristics of the gain medium and can be depicted as $I_s = h\upsilon/\sigma\tau$ for a four-level system, where $h\upsilon$ is photon energy, σ is emission cross section for stimulated emission, and τ represents spontaneous decay time of the upper laser level.

Then, for power transmission in the resonant cavity, the transmission loss can be determined by the power difference between the two planes, and the power on a plane is the integral of the power intensity distribution concerning the plane area. Thus, the propagation loss δ_{qq+1} between the plane q and $q+1$ can be figured out as [23], [26]

$$\delta_{qq+1} = \frac{\iint_S |U_q|^2 \, ds - \iint_S |U_{q+1}|^2 \, ds}{\iint_S |U_q|^2 \, ds}, \tag{22}$$

where q is the indices of the planes in Fig. 6, $q = 1, 2, 3, 4$. Thus, the transfer factors V_{12} (from $R1$ to S_{ex}), V_{23} (from S_{ex} to $R2$), V_{34} (from $R2$ to S_{ex}) and V_{41} (from S_{ex} to $R1$) can be derived from (22) and [19] as

$$V_{qq+1} = 1 - \delta_{qq+1} = \frac{\iint_S |U_{q+1}|^2 \, ds}{\iint_S |U_q|^2 \, ds}. \tag{23}$$

Afterwards, in "Power Output," according to "Circulating Power Model" of laser in [20] and the "Output Power of Laser Resonators" in [19], the output beam power of RBC system with external object invasion can be expressed as [19], [20]

$$P_{\text{out}} = A_b I_s \frac{(1-R_2)V_{12}V_{23}}{1-R_2V+\sqrt{R_2\,V}\left(\frac{1}{V_{12}V_{23}V_S}-V_S\right)} \times \left(g_0\ell - |\ln\sqrt{R_2V_S^2V}|\right), \tag{24}$$

where A_b is the spot size of the resonant beam on the gain medium, and the radius of the resonant beam is defined as the radius at which the intensity on the input reflector is $1/e^2$ of its peak value on the axis [20]. R_2 is the reflectivity of the output reflector $R2$. V_S is the transfer factor of the gain medium, and V is the transfer factor of a round-trip transmission. Besides, form (20) and (21), the small signal gain $g_0\ell$ can be calculated as

$$g_0\ell = \frac{\eta_{excit}P_{in}}{AI_s}. \tag{25}$$

Finally, the output beam power P_{out} can be converted into output electric power P_e with PV panel in the receiver [12]

$$P_e = P_{out}\eta_{pv}, \tag{26}$$

where η_{pv} is the conversion efficiency of the PV panel. The output electric power is used for charging electronic devices.

C. Irradiance Calculation Model

Based on the "Circulating Power Model," the conversion of beam power from invading object aperture to output reflector $R2$ is [19]

$$P_{ex}^{+}V_{23}(1-R_2) = P_{out}, \tag{27}$$

where P_{ex}^{+} is the forward power on the invading object aperture. Hence, P_{ex}^{+} can be derived from (27) as

$$P_{ex}^{+} = \frac{P_{out}}{V_{23}(1-R_2)}. \tag{28}$$

Then, the power on the invading object aperture is equal to the integral value of the power density on the surface as [19]

$$P_{ex}^{+} = I_{2\,m}^{+}\iint_{S_{ex}} i_2\,(x_2,y_2)\,ds, \tag{29}$$

where $I_{2\,m}^{+}$ represents the maximum forward power density on the invading object plane, and $i_2(x_2,y_2)$ is the normalized distribution of forward power density on the invading object plane from "Electromagnetic Field Analysis". Combined with (28) and (29), the forward maximum power density can be depicted as

$$I_{2\,m}^{+} = \frac{P_{out}}{V_{23}(1-R_2)\iint_{S_{ex}} i_2\,(x_2,y_2)\,ds}. \tag{30}$$

Thus, substitute (30) into (5), the maximal forward irradiance I_2^{+} on the invading object can be expressed as

$$I_2^{+} = max\left(I_{2\,m}^{+}(z)i_2(x_2,y_2,z)\right) \tag{31}$$

TABLE I
PARAMETERS OF THE RBC SYSTEM

Symbol	Parameter	Value
a	Input/Output reflector radius	6*mm*
L	Transmission distance (Cavity length)	5*m*
R_1	Input reflector reflectivity	100%
R_2	Output reflector reflectivity	50%
r_m	Gain medium radius	6*mm*
η_{pv}	PV plane conversion efficiency	40%
λ	Resonant beam wavelength	1064*nm*

where $max()$ is used to obtain the maximum value of the forward irradiance on the invading object.

Similarly, the maximum backward power density $I_{2\,m}^{-}$ on the invading object plane is

$$I_{2\,m}^{-} = \frac{P_{out}V_{34}}{(1-R_2)\iint_{S_{ex}} i_4\,(x_4,y_4)\,ds}, \tag{32}$$

where V_{34} is the transfer factor from the output reflector to the invading object plane, and $i_4(x_4,y_4)$ is the normalized distribution of backward power density. In addition, the maximal backward irradiance of the invading object can be deduced from (31) and (32) as

$$I_2^{-} = max\left(I_{2\,m}^{-}(z)i_4(x_4,y_4,z)\right). \tag{33}$$

Therefore, the maximum irradiance I on the invading object can be derived from (4), (31), and (33).

Finally, we can determine the safety level of the RBC system according to the I_{MPE} in the "Safety of laser products IEC $60825-1$". For example, if the irradiance on the invading object I is less than $I_{MPE} = 1$ W/cm^2 of the skin safety, we confirm that the RBC system can realize the skin-safe wireless power transmission.

IV. NUMERICAL ANALYSIS

In this section, we will depict the inherent safety of the RBC system numerically based on the analytical model. If the external object invades the resonant cavity, the output beam and electric power of the RBC system, and the irradiance on the invading object will be analyzed to explain the effect of invasion. Then, to illustrate the superiority of RBC system safety, we will compare the irradiance on the invading object in the RBC system with the laser charging system under the same object invasion situation.

A. Parameters Setting

In this subsection, we demonstrate the parameters in numerical analysis for "Electromagnetic Field Analysis," "Circulating Power Model" and "Irradiance Calculation Model".

At first, the parameters of the RBC system are shown in Table I. The input reflector $R1$ and output reflector $R2$ are plane mirrors with equal radius a. A thin crystal Nd:YVO_4 is used as the gain medium, which is attached to the input reflector. The radius of the gain medium r_m is equal to that of the reflectors, i.e., $r_m = a$. Besides, the conversion efficiency of the PV panel η_{pv} represents the percentage of the output beam power converted to electric power. The size of external objects we study in this paper is much larger than that of the reflectors.

TABLE II
PARAMETERS FOR FFT-BASED CALCULATION AND FOX-LI NUMERICAL ITERATION METHOD

Symbol	Parameter	Value
G_R	Input/Output reflector expand factor	4
G_{ex}	External object plane expand factor	2
S_N	Sampling number	2048
N_{Itr}	Iteration number	300

TABLE III
PARAMETERS FOR CIRCULATING POWER MODEL

Symbol	Parameter	Value
I_s	Saturation intensity	$1260W/cm^2$
η_{excit}	Excitation efficiency	72%
V_s	Transfer factor in gain medium	99%
P_{eno}	Output electric power without invasions	$1W$

For intra-cavity electromagnetic field analysis, we adopt the FFT-based numerical calculation to obtain the field distribution on the observation window of the invading object plane after a round-trip propagation. The observation window of the invading object plane is twice the input/output reflector. To avoid aliasing effects in FFT, the computation window length of $2Gr$ is defined as the length of zero-padded aperture, where r is the radius of the input/output reflector or external object observation window, and G represents the expand factor. G_R and G_{ex} are the expand factor of reflectors and external object observation window. Besides, the sampling number is generally a power of 2. With the "Fox-Li" numerical iteration method, a steady-state can be formed in the resonator cavity when the iteration number N_{Itr} reaches 300 [30]. The detailed parameters are shown in Table II.

For circulating power transmission, the parameters in equation (24) are shown in Table III. To charge high-power mobile devices, such as mobile phones, we assume that the RBC system steadily outputs 1 W electric power without external object invasion. I_s, η_{excit}, and V_s are determined by the physical properties of the gain medium.

B. Analysis of Irradiance on Intra-Cavity Invading Object

As shown in Fig. 4, we assume that the external object is perpendicular to the optical axis and invades from a distance of radius a away from the resonant cavity until the input/output reflector is completely covered. That is, the invasion position of external object d, which is defined as the abscissa of the junction of the invading object and the resonant beam, changes from 0.012 m ($2a$) to -0.006 m ($-a$). That is, the horizontal coordinate from right to left shows the invasion of an external object into the resonant cavity from the distance of $d = 0.012$ m. $d = 0$ m is the abscissa origin of the input/output reflector depicted in Fig. 4.

Besides, z is the coordinate of the external object invasion position on the z-axis shown in Fig. 5, i.e., the position on the optical axis (the line connecting the centers of the input and output reflectors). For example, L is 5 m, $z = L/2$ means that the external object invades the resonant cavity in the midpoint of resonant cavity. That is, the coordinate on z-axis of invasion position is 2.5 m.

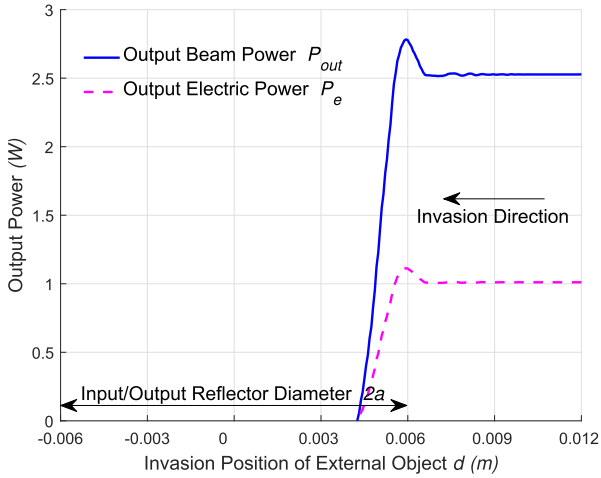

Fig. 8. Output beam and electric power versus of invasion position of external object ($z = L/2$).

To illustrate the effect of external object invasion on RBC system performance, we at first analyze the changes of output power, intra-cavity power, irradiance as the object invades at the mid-point of the resonant cavity (i.e., the z-axis coordinates of the external object plane $z = L/2$). Then, to determine the safety level of RBC system with FP cavity, we demonstrate the irradiance on the external object as it invades at any position on the z-axis.

1) Irradiance Calculation on the Object Invading At $z = L/2$: The changes of the output beam power P_{out} with the external object invasion are depicted in Fig. 8. If the invading object is far away from the resonator (i.e., the input/output reflectors are not shielded by invading object, $d > 0.006$ m), the output beam power is constant at 2.5 W. As the invading object approaches the resonant cavity ($d \approx 0.006$ m), the output beam power first increases and then decreases sharply to 0 W as the invasion position d changes to 0.0043 m. The output beam power of 0 W means that the resonant beam is interrupted due to the external object invasion, and the energy transmission ceased.

According to (26), the output electric power P_e is linearly correlated with the output beam power P_{out}. Thus, P_e has the same variation trend as P_{out} in Fig. 8. Besides, if the external object is far away from the resonant cavity, the out electric power is stable at 1 W, which is equal to the electric power without external object invasion. Similarly, the beam power in the middle of the resonant cavity based on (24), (28), and (32) is presented in Fig. 9.

In addition, the reasons for the increase in output power and intra-cavity power with the invasion position $d \approx 0.006$ m can be derived from Fig. 9. A_b/A is the ratio of the spot size of resonant beam to the cross-sectional area of the gain medium, which represents the degree of overlap between the resonator mode and the gain distribution in space. That is, the increase in A_b/A means that the gain area used for pumping is increased, allowing a greater amount of resonant beam energy to be stimulated out. As illustrated in [31], the energy in the resonant cavity with plane mirrors is concentrated around the optical axis, and the beam spot size on the gain medium is small and

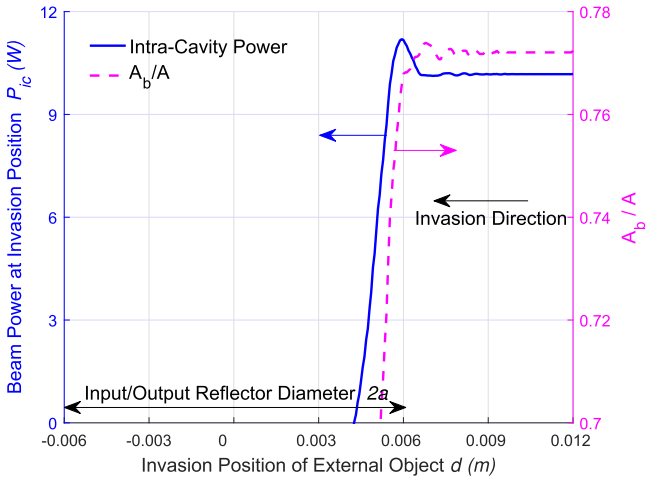

Fig. 9. Intra-cavity beam power and A_b/A versus the invasion position of external object ($z = L/2$).

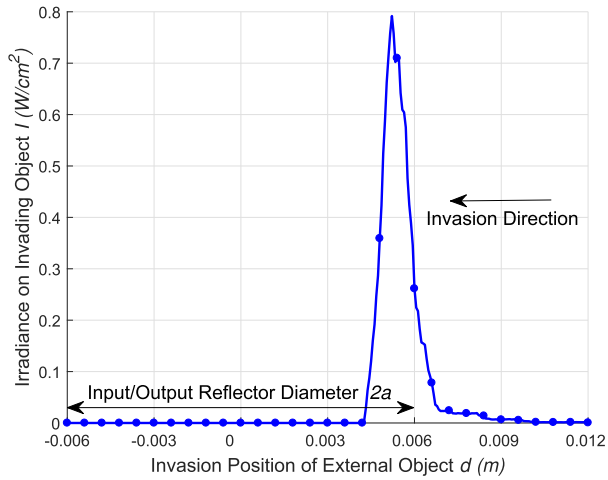

Fig. 10. Irradiance on invading object versus invasion position of external object ($z = L/2$).

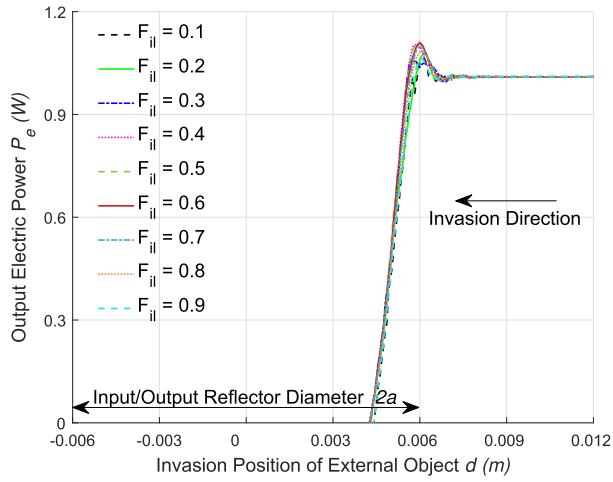

Fig. 11. Output electric power versus invasion position of external object (Invasion at any position on z-axis).

regular. As the invading object approaches the edge of resonant cavity ($d \approx 0.006$ m), the beam energy distribution spreads out to the border sides due to the diffraction effect brought by the invading object. Therefore, the beam spot size A_b on the gain medium increases. Afterwards, as the external object invades the cavity ($d < 0.006$ m), the external object aperture compresses the beam and A_b decreases. Combining (24), with the change of A_b/A, the output power starts steadily, then increases to the peak, and finally decreases to 0 with the invasion of an external object.

To determine the safety level of the RBC system, we evaluated the maximum irradiance I on the invading object during invasion. In Fig. 10, as the external object gradually invades until completely covers the input/output reflector (i.e., d gradually decreases from to -0.006 m), the irradiance on invading object first increases and then decreases to 0 W/m^2. Since the transmitted energy is concentrated with the resonant beam, the irradiance on the invading object is 0 W/m^2 as it is far away from the resonant cavity ($d > 0.006$ m). As invasion position d decreases, the irradiance gradually increases to the maximum value of 0.7917 W/cm^2. Afterwards, the irradiance I decreases to 0 W/m^2 with the resonant beam attenuation. Finally, the WPT is interrupted as $d = 0.0043$ m.

Since the maximum irradiance during the invasion is about 0.7917 W/cm^2, which is below the MPE of skin safety 1 W/cm^2, the RBC system can be determined as skin-safe with external objects invasion in the middle of the resonant cavity.

2) Irradiance Calculation on the Invading Object At Any Locations on Z-Axis: Based on the analysis of the invasion in the middle of the resonator, we analyze the safety of the RBC system by calculating the irradiance on the invading object during its invasion at representative locations inside the resonant cavity.

We denote F_{il} as the ratio of the distance between the invading object and the transmitter to the cavity length, i.e., $F_{il} = z/L$. That is, F_{il} represents the locations of external object invasion on the z-axis. For example, when $F_{il} = 0.1$, the external object invades the resonant cavity at a distance of 0.5 m from the transmitter with 5 m cavity length.

The changes of output electric power P_e with the external object invasion at the positions $F_{il} = 0.1 \sim 0.9$ are shown in Fig. 11. Similar to the invasion in the middle of the resonator (i.e., $F_{il} = 0.5$), the output electric power first increases and then decreases as d gradually decreases. The output electric power P_e is 0 W as the resonant beam is interrupted. Besides, the small data fluctuations in output electric power are shown due to the wave nature of resonant beam [19].

Moreover, the irradiance on the invading object is depicted in Fig. 12. As invasion position d decreases from 0.012 m to -0.006 m, the irradiance on invading object shows an uptrend from 0 W/cm^2 to the maximum value and then reduces to 0 W/cm^2. In addition, the irradiance with different F_{il} is various before the beam is cut off. In this process, the maximum irradiance is about 0.8052 W/cm^2, which is below the MPE of skin safety 1 W/cm^2. Thus, the RBC system is safe for human skin if the external object invades the resonant cavity at any location on the z-axis.

In summary, based on the numerical analysis, the irradiance on the invading object at any position on the z-axis in the resonant

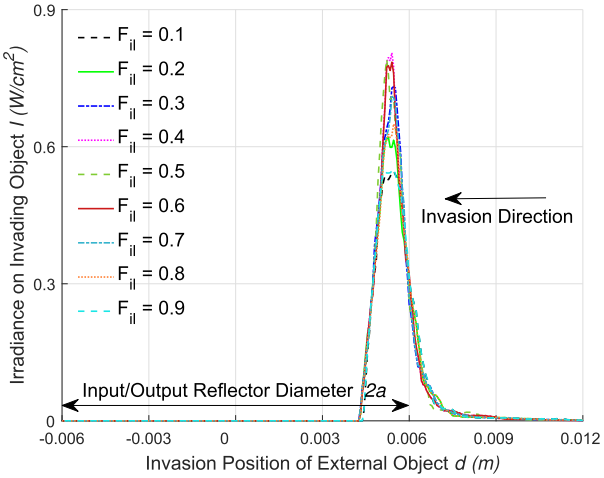

Fig. 12. Irradiance on external object versus invasion position of external object (Invasion at any position on z-axis).

cavity can be obtained. Moreover, the skin safety of the RBC system with FP cavity has been verified.

C. Irradiance on the Invading Object in RBC System and Laser Charging System

To distinctly illustrate the safety feature of the RBC system, we compared the electromagnetic field distribution on the output reflector and irradiance on the intra-cavity invading object (RBC system) and extra-cavity invading object (laser charging system). The invasion process is shown in Fig. 3, where the external object invades the RBC system at the midpoint of cavity (i.e., $F_{il} = 0.5$).

The changes of field distribution on the output reflector with the external object invasion are depicted in Fig. 13. In Fig. 13(a) and (b), the yellow solid circle represents the unoccluded area of reflectors from the left view of Fig. 4, while the other indicates the occluded area due to the external object invasion. As d decreases, the occluded area gradually expands until occupies the entire reflector.

Afterwards, if the external object invades the transmission path (i.e., resonant beam) of RBC system, the beam field on the output reflector gradually reduces with the decrease of d, as the object invasion weakens the gain amplification of resonant beam (Fig. 13(c), (d)). However, if the external object invades the transmission path (i.e., laser) of laser charging system, the invasion doesn't affect the intra-cavity gain amplification but only occludes the laser beam. The field distribution on the output reflector remains unchanged as d decreases (Fig. 13(e), (f)).

The comparison of irradiance on the invading object is shown in Fig. 14. We found that if the invading object is far away from the resonant beam ($d > 0.006$ m), the irradiance of the object in intra-cavity and extra-cavity is 0 W/cm^2. As d decreases and begins to cover the reflector ($d < 0.006$ m), the irradiance on the invading object increases. Since the extra-cavity laser will not be interrupted if occluded by the invading object, the irradiance on the object is greater than 0 W/cm^2 in the process of the external object invasion, and the irradiance is the largest when the object

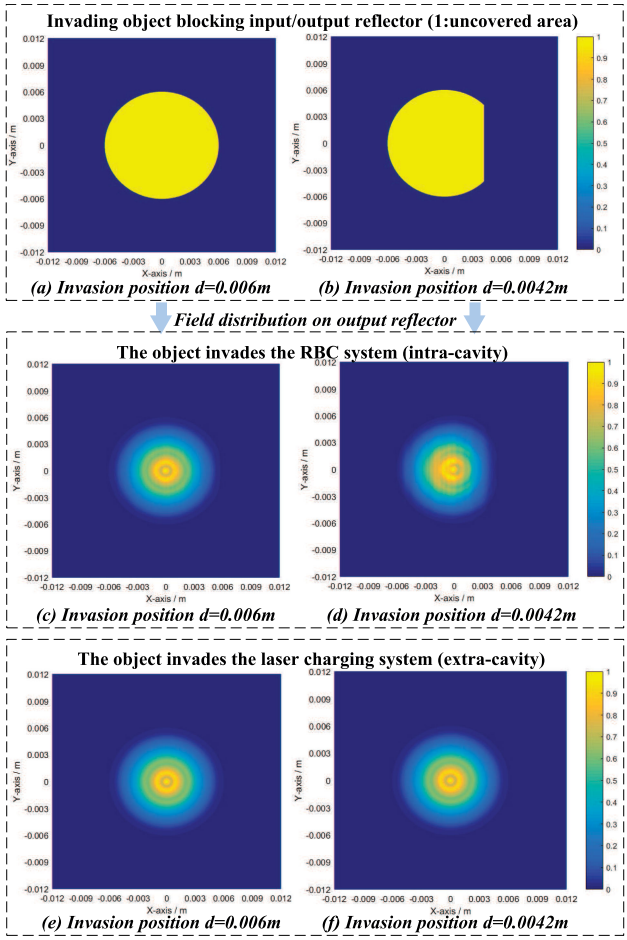

Fig. 13. Field distribution on the output reflector with the intra-cavity and extra-cavity invasions.

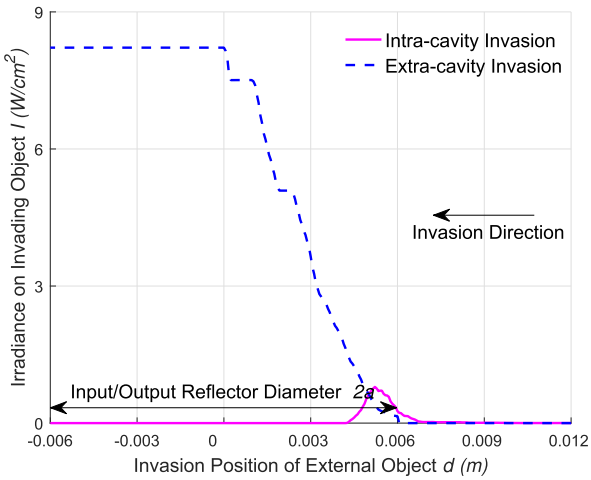

Fig. 14. Comparison of the irradiance on the invading object between RBC system and laser charging system.

reaches the optical axis (i.e., the connection of centers of the input and output reflectors). Moreover, if $d < 0$ m, the irradiance on the invading object is maintained at the maximum value since the object is irradiated by the center of the laser beam.

Afterwards, if the invading object is near the resonant cavity of RBC system $d \approx 0.006$ m, the irradiance on the intra-cavity invading object is larger than that of the extra-cavity invading object as the intra-cavity invading object affects the gain amplification. As d decreases, the irradiance on the extra-cavity invading object is larger than that of intra-cavity invading object and exceeds the MPE of skin safety (1 W/cm^2). Besides, the maximum of the irradiance on the extra-cavity invading object 8.2176 W/cm^2 is about 10 times greater than that of the irradiance on the intra-cavity invading object 0.8052 W/cm^2. Therefore, the safety of the RBC system significantly outperforms the laser charging system.

In conclusion, we can reach summaries as follows based on the numerical analysis: i) According to the analytical model, the irradiance on the invading object at any position in resonant cavity of RBC system can be calculated as the object invades the cavity; ii) The RBC system with FP cavity, 5 m transmission distance and 1 W output electric power is skin safe through the analysis of irradiance; and, iii) Compared with the laser charging system, the advantage over safety of RBC system is evident.

V. Conclusions and Discussions

A. Conclusions

In this paper, we revealed that the Resonant Beam Charging (RBC) system with a Fabry-Pérot (FP) cavity can realize skin-safe, long-range, and high-power Wireless Power Transfer (WPT). We first described the system dynamic response mechanism if the external object invades the resonant cavity. Then, we established the analytical model based on electromagnetic field analysis to calculate the irradiance on the invading object. Finally, the numerical analysis illustrated that the RBC system with FP cavity, 5 m cavity length, and 1 W output electric power is human-skin safe, and the irradiance on the invading object is only $1/10$ of the comparable laser charging system.

B. Discussions

Several topics are worthy of further study in the future: i) safety improvement of WPT with different RBC system parameters (e.g. reflector parameters, cavity length); ii) influences of the external object moving speed on safety; iii) safety analysis of RBC system based on a different structure, e.g. complex resonant cavity; and, iv) transmission and safety analysis in the resonant beam communication (RBCom) system and simultaneous wireless information and power transfer (SWIPT) system.

To verify the practicality of the proposed analytical model and numerical analysis, we will carry out experiments in future research and validate the experimental results against the theoretical analysis. The experiment for verifying RBC safety can be assigned as:

Based on Fig. 2, we design the experimental platform of the RBC system with 5 m transmission distance and 1 W output electric power. Afterwards, we use a blade to gradually invade the resonator in different positions for analyzing each performance metric. During the blade invasion, at first, the changes of output power are tested and compared with data in Fig. 11; then, the field distributions on the output reflector are detected using the beam profiler and compared with field distributions shown in Fig. 13(c), (d); finally, the intra-cavity beam at the invasion location is induced out of the cavity onto the power probe or the beam profiler for roughly measuring the beam power and field distribution on the invading object plane, and the measured data is compared with the irradiance in Fig. 12. We consider the proposed analytical model and numerical simulation to be valid if the experimental results match the numerical results with a certain error for the same system structural parameters.

References

[1] Q. Wu *et al.*, "Cognitive Internet of Things: A new paradigm beyond connection," *IEEE Internet Things J.*, vol. 1, no. 2, pp. 129–143, Apr. 2014.

[2] S. Fu, Y. Tang, N. Zhang, L. Zhao, S. Wu, and X. Jian, "Joint unmanned aerial vehicle (UAV) deployment and power control for Internet of Things networks," *IEEE Trans. Veh. Technol.*, vol. 69, no. 4, pp. 4367–4378, Apr. 2020.

[3] M. Sinaie, P. Lin, A. Zappone, P. Azmi, and E. A. Jorswieck, "Delay-aware resource allocation for 5G wireless networks with wireless power transfer," *IEEE Trans. Veh. Technol.*, vol. 67, no. 7, pp. 5841–5855, Jul. 2018.

[4] J. Shao, R. Lin, F. C. Lee, and D. Chen, "Characterization of EMI performance for hard and soft-switched inverters," in *Proc. 15th Annu. IEEE Appl. Power Electron. Conf. Expo.*, Los Angeles, USA, Feb. 2000, pp. 1009–1014.

[5] I. C.on non-ionizing radiation protection, "ICNIRP guidelines on limits of exposure to laser radiation of wavelengths between 180 nm and 1000 m," *Health Phys.*, vol. 105, no. 3, pp. 271–295, Sep. 2013.

[6] G. Monti *et al.*, "EMC and EMI issues of WPT systems for wearable and implantable devices," *IEEE Trans. Electromag. Compat.*, vol. 7, no. 1, pp. 67–77, Jun. 2018.

[7] S. Y. Jeong, H. G. Kwak, G. C. Jang, and C. T. Rim, "Living object detection system based on comb pattern capacitive sensor for wireless ev chargers," in *Proc. IEEE Annu. Southern Power Electron. Conf.*, Auckland, New Zealand, Dec. 2016, pp. 1–6.

[8] H. Zhai, H. K. Pan, and M. Lu, "A practical wireless charging system based on ultra-wideband retro-reflective beamforming," in *Proc. IEEE Antennas Propag. Soc. Int. Symp.*, Toronto, ON, Canada, Jul. 2010, pp. 1–4.

[9] V. Iyer, E. Bayati, R. Nandakumar, A. Majumdar, and S. Gollakota, "Charging a smartphone across a room using lasers," *Proc. ACM Interact. Mob. Wearable Ubiquitous Technol.*, vol. 1, no. 4, pp. 143: 1–21, Jan. 2018.

[10] Q. Liu *et al.*, "Charging unplugged: Will distributed laser charging for mobile wireless power transfer work?," *IEEE Veh. Technol. Mag.*, vol. 11, no. 4, pp. 36–45, Dec. 2016.

[11] W. Fang, Q. Zhang, Q. Liu, J. Wu, and P. Xia, "Fair scheduling in resonant beam charging for IoT devices," *IEEE Internet Things J.*, vol. 6, no. 1, pp. 641–653, Feb. 2019.

[12] Q. Zhang, W. Fang, Q. Liu, J. Wu, P. Xia, and L. Yang, "Distributed laser charging: A wireless power transfer approach," *IEEE Internet Things J.*, vol. 5, no. 5, pp. 3853–3864, Oct. 2018.

[13] Q. Zhang, W. Fang, M. Xiong, Q. Liu, J. Wu, and P. Xia, "Adaptive resonant beam charging for intelligent wireless power transfer," *IEEE Internet Things J.*, vol. 6, no. 1, pp. 1160–1172, Feb. 2019.

[14] W. Fang, Q. Zhang, M. Liu, Q. Liu, and P. Xia, "Earning maximization with quality of charging service guarantee for IoT devices," *IEEE Internet Things J.*, vol. 6, no. 1, pp. 867–877, Feb. 2019.

[15] Wi-charge, "Is IR power delivery safe?," Jun. 2020. [Online]. Available: https://wi-charge.com/is-ir-power-delivery-safe/

[16] I. E. Commission, "Safety of laser products-part 1: Equipment classification and requirements," IEC 60825–1, 2014.

[17] T. Kirubarajan, P. R. P. Hoole, S. R. H. Hoole, and K. Kiridharan, "Electromagnetic field computation and electromagnetic signal processing," *IEEE Trans. Magn.*, vol. 31, no. 3, pp. 1956–1959, May 1995.

[18] Wikipedia, "Signal," Mar. 2021. [Online]. Available: https://en.wikipedia.org/wiki/Signal

[19] N. Hodgson and H. Weber, *Laser Resonators and Beam Propagation: Fundamentals, Advanced Concepts, Applications*. Berlin, Heidelberg, Germany: Springer, 2005.

[20] W. Koechner, *Solid-State Laser Engineering*. Berlin, Heidelberg, Germany: Springer, 2013, vol. 1.

[21] S. Nordebo and M. Gustafsson, "Statistical signal analysis for the inverse source problem of electromagnetics," *IEEE Trans. Signal Process.*, vol. 54, no. 6, pp. 2357–2361, Jun. 2006.
[22] H. Haken, *Laser Theory*. Berlin, Heidelberg, Germany: Springer, 1970.
[23] J. Gordon and H. Kogelnik, "Equivalence relations among spherical mirror optical resonators," *Bell Syst. Tech. J.*, vol. 43, no. 6, pp. 2873–2886, May 1964.
[24] D. Hofer and B. G. Zagar, "A numerical approximation of the huygens-fresnel integral-simulations of a rough wetting problem," *Measurement*, vol. 46, no. 8, pp. 2828–2836, May 2013.
[25] T. Teperik, A. Archambault, F. Marquier, and J.-J. Greffet, "Huygens-fresnel principle for surface plasmons," *Opt. Exp.*, vol. 17, no. 20, pp. 17483–17490, Sep. 2009.
[26] T. Li, "Diffraction loss and selection of modes in maser resonators with circular mirrors," *Bell Syst. Tech. J.*, vol. 44, no. 5, pp. 917–932, May 1965.
[27] H. Kortz and H. Weber, "Diffraction losses and mode structure of equivalent TEM_{00} optical resonators," *Appl. Opt.*, vol. 20, no. 11, pp. 1936–1940, Jun. 1981.
[28] J. Cooley, P. Lewis, and P. Welch, "Application of the fast Fourier transform to computation of Fourier integrals, Fourier series, and convolution integrals," *IEEE Trans. Audio Electroacoust.*, vol. 15, no. 2, pp. 79–84, Jun. 1967.
[29] F. Shen and A. Wang, "Fast-Fourier-transform based numerical integration method for the Rayleigh-Sommerfeld diffraction formula," *Appl. Opt.*, vol. 45, no. 6, pp. 1102–1110, Feb. 2006.
[30] A. G. Fox and T. Li, "Resonant modes in a maser interferometer," *Bell Syst. Tech. J.*, vol. 40, no. 2, pp. 453–488, Oct. 1961.
[31] S. R. Barone, "Resonances of the Fabry-Perot laser," *J. Appl. Phys.*, vol. 34, no. 4, pp. 831–843, Sep. 1963.

Wen Fang received the B.E. degree in computer science and technology from the Shandong University of Science and Technology, Qingdao, China, in 2017. She is currently working toward the Ph.D. degree with the College of Electronics and Information Engineering, Tongji University, Shanghai, China. Her research interests include wireless power transmission, development of remote wireless charging technology, and Internet of Things.

Hao Deng received the B.S. and Ph.D. degrees from the Department of Physical Electronics, University of Electronic Science and Technology, Chengdu, China, in 2007 and 2015, respectively. From 2017 to 2020, he was a Postdoctoral Research Fellow with the College of Electronics and Information Engineering, Tongji University, Shanghai, China. Since 2020, he has been a Lecturer with the School of Software Engineering, Tongji University. His research interests include optical critical dimension measurement for semiconductors, wireless power transfer, and Internet of Things.

Qingwen Liu (Senior Member, IEEE) received the B.S. degree in electrical engineering and information science from the University of Science and Technology of China, Hefei, China, in 2001, and the M.S. and Ph.D. degrees from the Department of Electrical and Computer Engineering, University of Minnesota, Minneapolis, MN, USA, in 2003 and 2006, respectively. He is currently a Professor with the College of Electronics and Information Engineering, Tongji University, Shanghai, China. His research interests include wireless power transfer and Internet of Things.

Mingqing Liu received the B.S. degree in computer science and technology from Northwest A& F University, Xianyang, China, in 2018. She is currently working toward the Ph.D. degree with the College of Electronics and Information Engineering, Tongji University, Shanghai, China.

Her research interests include wireless power transfer, development of remote wireless charging technology, and Internet of Things.

Qingwei Jiang received the B.S. degree in internet of things engineering from the Jinan University, Guangzhou, China, in 2020. He is currently working toward the Ph.D. degree with the College of Electronics and Information Engineering, Tongji University, Shanghai, China. His research interests include wireless power transfer and Internet of Things.

Liuqing Yang (Fellow, IEEE) received the Ph.D. degree in electrical and computer engineering from the University of Minnesota, Minneapolis, MN, USA, in 2004. She is currently a Professor with the University of Minnesota. She has authored or coauthored more than 330 journal and conference papers, four book chapters and five books in research field. which include communications and networking She is the Editor-in-Chief of the *IET Communications*, an Executive Editorial Committee Member of the IEEE TRANSACTIONS ON COMMUNICATIONS, and the Senior Editor of the IEEE TRANSACTIONS ON SIGNAL PROCESSING. She was also the Editor of the IEEE TRANSACTIONS ON WIRELESS COMMUNICATIONS, IEEE TRANSACTIONS ON INTELLIGENT TRANSPORTATION SYSTEMS, IEEE INTELLIGENT SYSTEMS, and *PHYCOM: Physical Communication*, and the program chair, track or symposium or TPC chair for many conferences. She was the recipient of the ONR Young Investigator Program (YIP) Award in 2007, and the NSF Faculty Early Career Development (CAREER) Award in 2009, the Best Paper Award at IEEE ICUWB'06, ICCC'13, ITSC'14, GLOBECOM'14, ICC'16, WCSP'16, GLOBECOM'18, ICCS'18 and ICC'19.

Georgios B. Giannakis (Fellow, IEEE) received the Diploma degree in electrical engineering from the National Technical University of Athens, Athens, Greece, in 1981. From 1982 to 1986, he was with the University of the Southern California, Los Angeles, CA, USA, where he received the M.Sc. and Ph.D. degrees in electrical engineering in 1983 and 1986, respectively.

From 1987 to 1998, he was with the University of Virginia, Charlottesville, VA, USA, and since 1999, he has been a Professor with the University of Minnesota, Minneapolis, MN, USA, where he holds an Endowed Chair of wireless telecommunications, University of Minnesota McKnight Presidential Chair of electrical and computer engineering, and is the Director of Digital Technology Center. He has authored or coauthored more than 450 journal papers, 750 conference papers, 25 book chapters, two edited books, and two research monographs (h-index 143) in his research field, which include communications, networking, and statistical signal processing. His current research interests include learning from big data, wireless cognitive radios, and network science with applications to social, brain, and power networks with renewables. He is the Co-Inventor of 32 patents issued. He was the Co-recipient of nine best paper awards from the IEEE Signal Processing (SP) and Communications (Com) Societies, including the G. Marconi Prize Paper Award in Wireless Communications. He is also a recipient of the Technical Achievement Awards from the SP Society (2000), from the EURASIP (2005), the IEEE ComSoc Education Award (2019), the Young Faculty Teaching Award, the G. W. Taylor Award for Distinguished Research from the University of Minnesota, and the IEEE Fourier Technical Field Award (inaugural recipient in 2015). He is a Fellow of the EURASIP, and has served IEEE holding number of posts, including a Distinguished Lecturer for the IEEE-SP Society.